Photocurrent Enhancement in Hybrid Nanocrystal Quantum-Dot *p-i-n* Photovoltaic Devices

S. Chanyawadee,[1] R. T. Harley,[1] M. Henini,[2] D. V. Talapin,[3] and P. G. Lagoudakis[1,*]

[1]*School of Physics and Astronomy, University of Southampton, Southampton, SO17 1BJ, United Kingdom*
[2]*School of Physics and Astronomy, University of Nottingham, Nottingham, NG7 2RD, United Kingdom*
[3]*Department of Chemistry, The University of Chicago, Chicago, Illinois 60637, USA*

(Received 6 August 2008; published 20 February 2009)

We fabricate a hybrid nanocrystal quantum-dot patterned *p-i-n* structure that utilizes nonradiative energy transfer from highly absorbing colloidal nanocrystal quantum dots to a patterned semiconductor slab to demonstrate a sixfold increase of the photocurrent conversion efficiency compared to the bare *p-i-n* semiconductor device.

DOI: 10.1103/PhysRevLett.102.077402 PACS numbers: 85.60.−q, 33.50.−j, 42.82.Fv, 71.35.−y

The physical advantage of organic semiconductors and colloidal nanocrystal quantum dots (NQDs) is the large light-absorption cross section. However, both material systems are plagued by low-charge-transfer efficiency that limits the overall power conversion efficiency of these materials in photovoltaic devices (PVs) when compared to silicon-based or epitaxial *p-n* junction PVs. In nature, funneling of energy between chromophores predominantly occurs through a nonradiative dipole-dipole coupling mechanism, first studied by Förster [1], that does not involve charge transfer or emission and absorption of photons between donor and acceptor and that can exceed the radiative energy transfer routinely used in phosphor light emitting devices. Experimental evidence of the above mechanism has been observed in hybrid semiconductor heterostructures under optical excitation between carriers in a single semiconductor quantum well and a vicinal layer of colloidal semiconductor quantum dots [2–4] or organic molecules [5–7]. Here, through reverse engineering we design and fabricate hybrid photovoltaic structures that utilize nonradiative energy transfer to extract carriers from colloidal NQDs and efficiently transfer them into a single-crystal *p-i-n* structure in a configuration that leads to strong enhancement of the measured photocurrent.

The heterostructure we investigate was grown by molecular beam epitaxy on a (100) GaAs substrate in a *p-i-n* configuration that consists of 20 periods of 7.5 nm thick GaAs quantum wells with 12 nm thick AlGaAs barriers [8]. The top contact of the structure is an open circular mesa. A scanning electron microscope image of the device is shown in Fig. 1(a). The heavy- and light-hole absorption peaks are observed from photocurrent measurements and are shown together with the quantum well photoluminescence (PL) in Fig. 1(c) at 25 K. Photocurrent measurements also reveal strong absorption from the topmost AlGaAs barriers around 585 nm. On this device we fabricate channels in a pattern of 80×80 μm^2 using a focused Ga^+ ion beam. The channels are 1.4 μm deep, 570 nm wide, and separated by 1.5 μm wide wires shown in the inset of Fig. 1(a). The hybrid configuration is then completed by drop casting an overlayer of colloidal NQDs on the patterned *p-i-n* structure. Colloidal NQDs are also deposited on a flat—not patterned—*p-i-n* structure that is used as a control sample for the demonstration of photocurrent enhancement due to nonradiative energy transfer. To minimize the effect of radiative energy transfer to the quantum wells from the quantum dots deposited on the top surface of the structure, we use CdSe/CdS colloidal NQDs with strongly detuned emission energy from the heavy- and light-hole absorption peaks of the quantum wells. The NQDs are grown using organometallic synthesis and are capped with hexadecylamine, tri-*n*-octylphosphine oxide, and tri-*n*-octylphosphine [9]. The fluorescence and absorption spectrum of the NQDs is shown in Fig. 1(c), and a schematic of the hybrid NQD patterned *p-i-n* structure is shown in Fig. 1(b), where the channels are sketched only partially filled with NQDs as observed from scanning electron microscopy of the hybrid structures (bottom right image of Fig. 1(a)].

The microstructuring of the *p-i-n* devices exposes the lateral side of the embedded quantum wells leading to formation of surface states that are known to trap quantum well carriers. The influence of nonradiative surface states on the quantum yield of the emission is accentuated in colloidal NQDs where the number of surface to bulk atoms in the crystal is increased. In the case of colloidal NQDs recent advances in synthetic chemistry allowed for passivation of the surface dangling bonds with appropriate organic ligands. Recently colloidal NQDs with quantum yields approaching 100% were reported [10]. Here we minimize the detrimental effect of surface states on the revealed quantum well facets by depositing colloidal NQDs with organic ligands that also passivate the surface states of the microstructured quantum wells. Although the nature of the passivations is not fully understood, the elimination of nonradiative surface states is confirmed from transient quantum well photoluminescence measurements. The quantum well photoluminescence decay of the patterned *p-i-n* structures with and without the colloidal NQDs is shown in Fig. 2(a). The patterned *p-i-n* structures are excited nonresonantly at 584 nm, and the photoluminescence dynamics are recorded using time-correlated

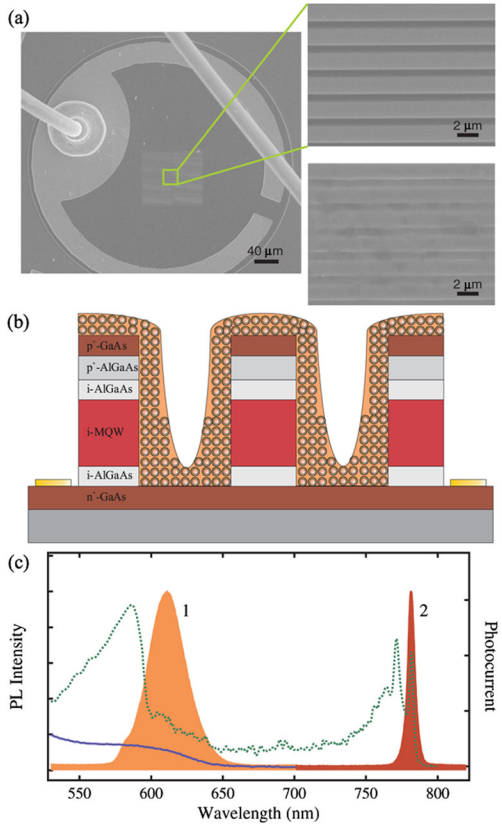

FIG. 1 (color online). (a) Scanning electron microscope images of the patterned *p-i-n* sample. The top and bottom right scanning electron microscope images are a magnification of the channels before and after the deposition of NQDs. (b) A schematic of the hybrid patterned device where the channels are partially filled with NQDs. (c) Spectral overlap of the hybrid NQD patterned *p-i-n* structure. The NQD fluorescence (in orange, labeled 1) and absorption (blue solid line) spectrum. The photoluminescence of the quantum wells (in red, labeled 2) and the photocurrent of the *p-i-n* device (green dotted line) that shows the heavy- and light-hole resonance.

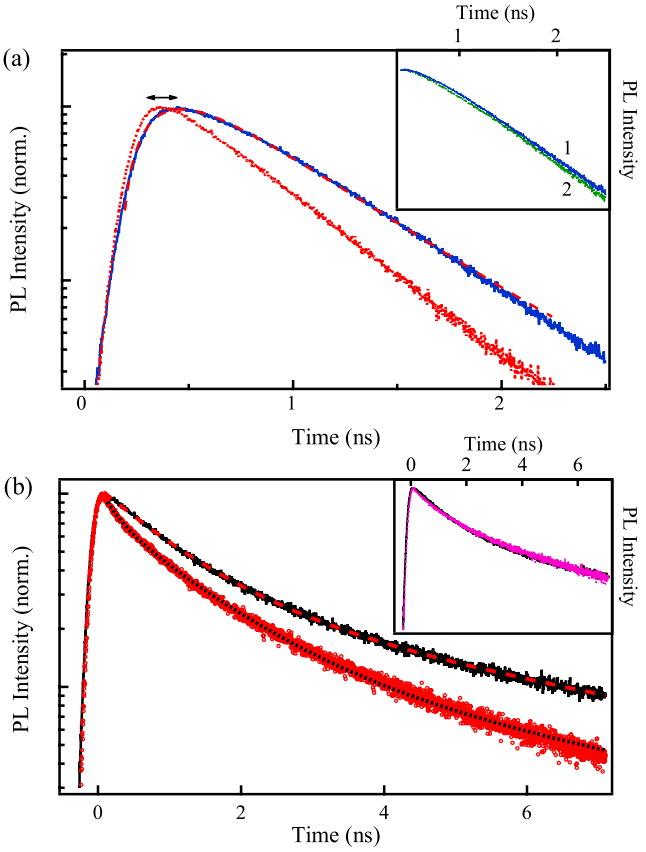

FIG. 2 (color online). Time resolved measurements of the hybrid NQD patterned *p-i-n* structure at 25 K. (a) Photoluminescence decay of the bare patterned *p-i-n* device before (red dotted line) and after (blue solid line) depositing NQDs. The left-right arrow points to the extended rise time in the hybrid patterned structure due to nonradiative energy transfer. The red dashed line is the fitting result of Eq. (1). Inset: the photoluminescence decay of the hybrid NQD patterned *p-i-n* structure (decay 1) and the photoluminescence decay of the flat *p-i-n* structure (decay 2). (b) Fluorescence decay of NQDs on a glass substrate (black solid line) and on the patterned *p-i-n* structure (red open circles). The red dashed and the black dotted lines are the biexponential fitting curves of the NQD fluorescence on a glass substrate and on the patterned *p-i-n* structure, respectively. Inset: the fluorescence decay of the NQDs on a glass substrate (black solid line) and on the unpatterned *p-i-n* device (pink dotted line).

single-photon counting and an avalanche photodiode that provides 40 ps resolution, while spectral filters are used to select the photoluminescence of the quantum wells only. The long tail of the photoluminescence decay ($t \geq 1$ ns) is fitted with an exponential curve, and the decay rate is estimated for both structures. The photoluminescence decay rate of the bare patterned structure is 20% faster compared to the decay rate of the hybrid patterned structure ($k_{\mathrm{QW}} = 2.13\ \mathrm{ns}^{-1}$, $k_{\mathrm{QW+QD}} = 1.78\ \mathrm{ns}^{-1}$), signifying the contribution of organic ligands on the surface of the colloidal NQDs in passivating the surface states of the patterned quantum wells [11]. Remarkably a comparison of the long tail of the photoluminescence decay of the hybrid patterned *p-i-n* structure and of the flat—control—sample, also plotted in the inset of Fig. 2(a), shows very similar transient decay curves (decay rates within 1% for $t \geq 1$ ns) suggesting that organic ligands can virtually eliminate any additional nonradiative recombination sites that occur from the patterning of the *p-i-n* structure.

The extended rise time of the hybrid patterned quantum wells compared to the bare patterned quantum wells indicated with a left-right arrow in Fig. 2(a) shows the onset of energy transfer from colloidal NQDs to the quantum wells. Colloidal NQDs deposited in the channels of the patterned quantum wells transfer energy in the adjacent structure both radiatively and nonradiatively. To characterize the efficiency of nonradiative energy transfer in the hybrid NQD patterned *p-i-n* structure, the fluorescence decay of colloidal NQDs in the hybrid structure and on a

glass substrate is measured using time-correlated single-photon counting and appropriate spectral filters. The NQDs are nonresonantly pumped at 400 nm, 100 fs pulses, and a 250 kHz repetition rate. Figure 2(b) shows the fluorescence decay of NQDs on a glass substrate and on the patterned *p-i-n* structure, and comparison of the two fluorescence decay curves clearly reveals the presence of an extra nonradiative energy transfer channel in the hybrid structure. Whereas on the glass substrate the fluorescence decay of NQDs is dominated by the radiative and any nonradiative recombination channels intrinsic to the NQDs, in the hybrid patterned structure nonradiative energy transfer to the patterned quantum wells contributes to the NQD fluorescence decay rate as an extra nonradiative channel. Thus the fluorescence decay rate of the NQDs in the hybrid structure is given by $k_H = k_{\mathrm{QD}} + k_{\mathrm{ET}}$ where k_{QD} and k_{ET} are the fluorescence decay rate of the NQDs and the nonradiative energy transfer rate, respectively. Since nonradiative energy transfer strongly scales with the separation distance between donor and acceptor, in the hybrid configuration only the NQDs deposited on the sides of the channels of the patterned structure transfer energy nonradiatively, and therefore we can assume that there are two kinds of NQDs in the ensemble, those that undergo nonradiative energy transfer and those that do not. The fluorescence decay of NQDs on a glass substrate, shown in Fig. 2(b), is dominated by a fast and a slow component that can be approximated with a biexponential fit also plotted in Fig. 2(b), with the fast decay rate $k_{\mathrm{QD}_1} = 0.9\ \mathrm{ns}^{-1}$ and the slow decay rate $k_{\mathrm{QD}_2} = 0.2\ \mathrm{ns}^{-1}$. The inset of Fig. 2(b) shows the fluorescence decays of the NQDs on an unpatterned *p-i-n* structure and on a glass substrate. The decay dynamics in both cases are virtually identical, which also suggests that interdot dynamics are unchanged on the glass substrate and the unpatterned *p-i-n* structures. The fluorescence decay of NQDs on the patterned structure can be more accurately described with $I(t) = \sum_{i=1,2} A_i e^{-k_{Hi}t} + \sum_{i=1,2} B_i e^{-k_{\mathrm{QD}i}t}$. The first two terms describe the decay dynamics of the NQDs that transfer energy to the patterned structure nonradiatively, and the last two terms describe the decay dynamics of the NQDs that do not transfer energy to the patterned structure nonradiatively. Since the energy transfer rate is proportional to the oscillator strength of the donor dipole, the ratio of the energy transfer rates corresponding to the transition dipoles of high and low oscillator strength scales approximately with the ratio of the fluorescence decay rates of the fast and slow components, respectively, $\frac{k_{\mathrm{QD}_1}}{k_{\mathrm{QD}_2}} = \frac{k_{\mathrm{ET}_1}}{k_{\mathrm{ET}_2}}$. This dependence also indicates that the contribution of the fast and slow components to the transient fluorescence, with and without nonradiative energy transfer, should remain unchanged. By taking these considerations into account we fit the fluorescence decay curve of the NQDs in the hybrid configuration, shown in Fig. 2(b), and obtain that the nonradiative energy transfer efficiency (η_{ET}) in the hybrid patterned configuration is 79% where $\eta_{\mathrm{ET}} = k_{\mathrm{ET}}/(k_{\mathrm{ET}} + k_{\mathrm{QD}})$. From the relative amplitude of the two subsets of NQDs it emerges that ~81% of the NQDs undergo nonradiative energy transfer as expected from a thin film of NQDs on the patterned structure.

The full potential of the investigated hybrid configuration can only be gauged by comparison of the photocurrent of the hybrid patterned and hybrid flat heterostructure. Both samples are optically excited at 400 nm, focused at a spot size smaller than the etched area of the patterned *p-i-n* structure, typically ~40 μm, and the generated photocurrent is measured using lock-in detection. The excitation wavelength is chosen so as to avoid nonlinear absorption of NQDs. Comparison of photocurrent measurements on the hybrid flat—control—device and on the hybrid patterned *p-i-n* structure, shown in Fig. 3, demonstrates a dramatic increase in the hybrid patterned device. In the flat—control—structure NQD fluorescence is absorbed at the topmost layer of the *p-i-n* device, and the measured photocurrent is almost unaffected by the overlayer of colloidal NQDs due to the short absorption length of the top layers of the device. This is due to the bending of the conduction band at the vicinity of the electrical contact that prevents the separation of the optically excited electron hole pairs at the top layer and therefore the generation of the photocurrent. In stark contrast, deposition of colloidal NQDs on the patterned structure dramatically increases the measured photocurrent, where lateral energy transfer can occur through the whole cross section of the microchannels. The photocurrent (I) of the control sample exhibits a linear dependence on the pump fluence (P), $I \propto a_C P$, where a_C is power conversion constant. In the case of the hybrid patterned structure we observe a ten-

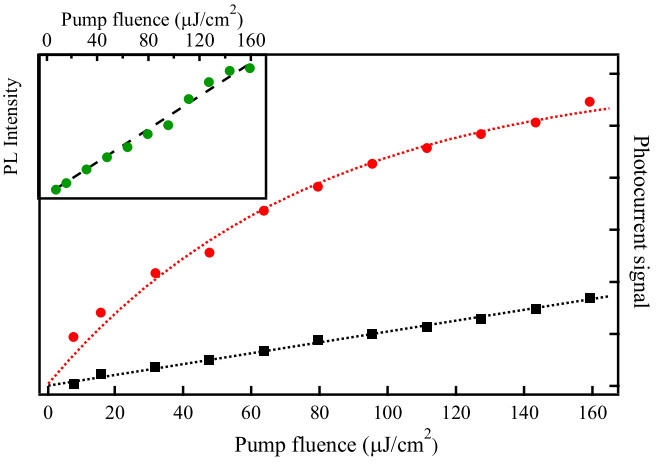

FIG. 3 (color online). Photocurrent of hybrid NQD *p-i-n* structure. Pump fluence dependence of photocurrent of the hybrid NQD flat quantum well structure (black squares) and of the hybrid NQD patterned *p-i-n* structure (red dots) at 25 K. Dotted red and black lines are fits to the photocurrent signal as described in the text. Inset: fluorescence intensity of NQDs versus pump fluence (green dots).

dency toward saturation for pump fluence higher than 60 $\mu J/cm^2$. It is possible that the photocurrent saturation in the hybrid patterned heterostructure is observed due to nonlinearities in the quantum wells such as excitation induced changes of the refractive index and nonlinear absorption [12,13]. We approximate the photocurrent of the hybrid patterned structure with $I = I_S(1 - e^{-a_H P})$, where I_S, $a_H^{-1} = 76.9\ \mu J/cm^2$ are the saturation photocurrent and threshold power, respectively. For pump fluence in the range of linear response of the hybrid structure, the ratio of the photocurrent conversion efficiency of the two devices is $(I_S a_H)/a_C = 6$. Clearly lateral energy transfer in the patterned configuration is improving the light to current conversion efficiency. We have confirmed that the photocurrent saturation is not due to nonlinearities on the NQD emission [14] since we observe a linear increase of the integrated NQD fluorescence for the same range of pump fluence, shown in the inset of Fig. 3, and that the photocurrent of the hybrid flat and the bare flat *p-i-n* structure is virtually identical within the absorption spectrum of the NQDs.

From the ratio of the nonradiative energy transfer rate to the NQD radiative rate we can estimate the contribution of the two processes in the increase of the measured photocurrent. The NQD radiative rate is given by $k_{\mathrm{rad}} = k_{\mathrm{QD}} Q_{\mathrm{ef}}$, where Q_{ef} is the quantum efficiency of the NQDs. For the NQDs used in this study $Q_{\mathrm{ef}} \cong 40\%$. From the transient fluorescence measurements we derive $\frac{k_{\mathrm{ET}}}{k_{\mathrm{QD}} Q_{\mathrm{ef}}} \cong 10$, which strongly suggests that the NQDs pump the *p-i-n* structure mostly through nonradiative energy transfer. To quantitatively describe the nonradiative energy transfer we use a kinetic model that can describe excitation dynamics in hybrid heterostructures [15]. The analytic solution of the hybrid NQD donor-QW acceptor system is given by

$$I(t) = \sum_{i=1,2} \frac{n_{\mathrm{QD}_i}(0) k_{\mathrm{ET}_i}}{k_{\mathrm{QW}} - k_{\mathrm{QD}_i} - k_{\mathrm{ET}_i}} (e^{-(k_{\mathrm{QD}_i} + k_{\mathrm{ET}_i})t} - e^{-k_{\mathrm{QW}} t}) + f(t), \quad (1)$$

where $n_{\mathrm{QD}_i}(0)$ is the initial population of the resonantly excited NQDs, $k_{\mathrm{QW}} = 2.1\ \mathrm{ns}^{-1}$ is photoluminescence decay rate of the quantum wells, and $f(t)$ is the direct optical pumping. This equation accurately describes the photoluminescence decay of the quantum wells. In Fig. 2(a), the photoluminescence decay of the quantum wells is superimposed with a fit of the above equation, where the only variable parameters are the initial populations $n_{\mathrm{QD}_i}(0)$ and ratio between direct optical pumping and indirect energy transfer from the NQDs. The best fit is obtained when 89% of the energy is injected into the QWs through nonradiative energy transfer from the NQDs in agreement with the qualitative estimation derived above for the ratio of the nonradiative energy transfer rate to the NQD radiative rate.

The hybrid *p-i-n* structure investigated in this report exemplifies the strength of nonradiative energy transfer in appropriately engineered hybrid photovoltaic devices for funneling energy between intrinsically different classes of semiconductors, while overcoming altogether the limitations imposed by the low-charge-transfer efficiency of highly absorbing compounds. Conclusive evidence of the transfer mechanism is produced by complementary measurements of the transient dynamics of the NQDs and the *p-i-n* structure. For this purpose, the characterization of the effect is studied at low temperatures in order to allow for sufficient photoluminescence quantum yield of the *p-i-n* device. The observed light to current conversion efficiency enhancement depends on temperature only through the scaling of the transfer mechanism between bound and free carrier pairs. Therefore the introduced hybrid configuration provides a new route for room temperature highly efficient photovoltaic devices. Whereas control over the growth and understanding of the dynamics of nonradiative energy transfer between QWs and NQDs or organic compounds has reached the maturity for the investigated configuration to demonstrate photocurrent enhancement compared to the bare *p-i-n* device, future studies will focus on bulk *p-i-n* and *p-n* structures and silicon-based PVs. Furthermore, this configuration is not limited to NQDs but is applicable to any solution-based highly absorbing semiconductor materials.

This work was partially supported by the EPSRC Grant No. EP/F013876/1 and the Royal Thai Government (S. C.).

*Corresponding author.
pavlos.lagoudakis@soton.ac.uk

[1] T. Förster, Ann. Phys. (Leipzig) **437**, 55 (1948).
[2] M. Achermann *et al.*, Nature (London) **429**, 642 (2004).
[3] S. Lu and A. Madhukar, Nano Lett. **7**, 3443 (2007).
[4] S. Rohrmoser *et al.*, Appl. Phys. Lett. **91**, 092126 (2007).
[5] G. Heliotis *et al.*, Adv. Mater. **18**, 334 (2006).
[6] S. Blumstengel *et al.*, Phys. Rev. Lett. **97**, 237401 (2006).
[7] G. Itskos *et al.*, Phys. Rev. B **76**, 035344 (2007).
[8] The top *p*-doped GaAs layer is 250 nm thick grown on a 500 nm thick layer of *p*-doped AlGaAs. The undoped AlGaAs buffer layers on both sides of multiple-quantum well structures are 100 nm thick.
[9] D. V. Talapin *et al.*, Nano Lett. **3**, 1677 (2003).
[10] X. Brokmann *et al.*, Phys. Rev. Lett. **93**, 107403 (2004).
[11] We have observed that not all kinds of surface ligands will reduce the nonradiative recombination rate of the patterned quantum well surface states and that some kinds (amines) will even increase the recombination rates.
[12] D. S. Chemla *et al.*, IEEE J. Quantum Electron. **20**, 265 (1984).
[13] T. Sizer *et al.*, IEEE J. Quantum Electron. **30**, 399 (1994).
[14] R. M. Kraus *et al.*, J. Phys. Chem. B **109**, 18 214 (2005).
[15] S. Chanyawadee *et al.*, Phys. Rev. B **77**, 193402 (2008).